Nanoscale Res Lett (2009) 4:97–105
DOI 10.1007/s11671-008-9208-3

NANO EXPRESS

Photodegradation of Pollutants in Air: Enhanced Properties of Nano-TiO_2 Prepared by Ultrasound

Giuseppe Cappelletti · Silvia Ardizzone · Claudia L. Bianchi · Stefano Gialanella · Alberto Naldoni · Carlo Pirola · Vittorio Ragaini

Received: 29 July 2008 / Accepted: 11 November 2008 / Published online: 25 November 2008

Abstract Nanocrystalline TiO_2 samples were prepared by promoting the growth of a sol–gel precursor, in the presence of water, under continuous (CW), or pulsed (PW) ultrasound. All the samples turned out to be made of both anatase and brookite polymorphs. Pulsed US treatments determine an increase in the sample surface area and a decrease of the crystallite size, that is also accompanied by a more ordered crystalline structure and the samples appear to be more regular and can be considered to contain a relatively low concentration of lattice defects. These features result in a lower recombination rate between electrons and holes and, therefore, in a good photocatalytic performance toward the degradation of NO_x in air. The continuous mode induces, instead, the formation of surface defects (two components are present in XPS Ti $2p_{3/2}$ region) and consequently yields the best photocatalyst. The analysis of all the characterization data seems to suggest that the relevant parameter imposing the final features of the oxides is the ultrasound total energy *per* volume (E_{tot}/V) and not the acoustic intensity or the pulsed/continuous mode.

G. Cappelletti (✉) · S. Ardizzone · C. L. Bianchi · A. Naldoni · C. Pirola · V. Ragaini
Department of Physical Chemistry and Electrochemistry, University of Milan, Via Golgi 19, 20133 Milan, Italy
e-mail: giuseppe.cappelletti@unimi.it

G. Cappelletti · S. Ardizzone · C. L. Bianchi · A. Naldoni · C. Pirola · V. Ragaini
Consorzio INSTM, Via Giusti 9, 50121 Florence, Italy

S. Gialanella
Department of Materials Engineering and Industrial Technologies, University of Trento, Via Mesiano 77, 38050 Trento, Italy

Keywords US-assisted synthesis · Nanostructured TiO_2 · Photocatalysis · NO_x degradation · Microstructural characterization

Introduction

The use of ultrasonic sources in environmental remediation has been extensively studied, both in combination with other processes and also by itself [1–4]. The principal mode of action of continuous ultrasound is the production of hydroxyl radicals from water sonolysis, that can promote the degradation process of pollutants.

Sonochemical processing to obtain materials with improved or unusual properties is, instead, relatively recent [5–11]. The chemical effect of ultrasound arises from acoustic cavitation, that is, the formation, growth, and implosive collapse of bubbles in a liquid. The implosive collapse produces high temperatures and pressures with localized hot spots, characterized by transient temperatures up to about 5000 K and pressures up to 1800 atm. The involved heating and cooling rates may be larger than 108 K s^{-1}. Nanoparticles showing a more uniform size distribution, higher surface area, a more controlled phase composition are some of the interesting features resulting from the application of sonication as a synthetic method.

The synthesis of TiO_2 with tailored features widens the field of applications of the semiconductor oxide, among which the photocatalytic processes aimed at degrading environmental pollutants [12–19]. It is well known that the morphology and structure of a nanosized material can deeply affect the semiconductor performance [14, 20]. Previously reported results [15, 16] have shown that the photocatalytic performance of TiO_2, in reactions performed both in water solution and in gas phase, is the result of a

complex balance between diverging effects (e.g., crystallinity, surface area) and that the surface state plays a key role in determining the kinetics of the relevant reactions.

Results present in the literature concerning the synthesis of TiO_2 assisted by US are rather difficult to rationalize since very different experimental conditions are adopted and the specific power of the US source is not reported in all cases. Meskin et al. [10] report the hydrothermal synthesis of TiO_2 in an autoclave, coupled with ultrasonic activation. The results demonstrate that ultrasonic activation markedly accelerates the crystallization rates and raises the rutile content with respect to the values obtained in synthesis carried out under identical conditions, but without sonication. Similarly, Arami et al. [8] produced nanostructured rutile with 15–20 nm crystallite size, which is usually difficult to be obtained at low temperatures, by simply treating in ultrasonic bath the product of dissolution of TiO_2 pellets in 10 M NaOH. Other authors, instead, observe opposite effects. Kim et al. [11] combine a short aging of a $TiCl_4$ hydro-alcoholic solution with a sonication treatment performed in a conventional low power sonifier. In this case US depresses rutile formation, induces smaller particle size and larger surface areas. Yu et al. [6] by a similar procedure based on the combination of a sol–gel synthesis with a treatment in a conventional ultrasonic bath, observe that ultrasonic irradiation enhances the crystallization rate of the TiO_2 gel.

Gedanken et al. [7, 9] report the beneficial effects of ultrasonic irradiation on the template synthesis of worm-like TiO_2 in presence of a long chain amine. The authors measured very high surface areas (853 $m^2\ g^{-1}$) for un-calcined products and a higher thermal stability of the mesoporous structures as compared to those samples that were not ultrasonically treated.

To gain some new evidence on the key role played by US in the formation and growth of nanocrystalline TiO_2, in the present work US treatments are applied during the aging of sol–gel precursors. Both continuous and pulsed US treatments are used. In the case of these latter treatments, both the on/off time and the power were modulated. To the authors best knowledge, no data are present in the literature so far concerning the use of pulsed US on the growth of TiO_2 particles. The structural and morphological features of the synthesized samples are investigated using different experimental techniques. The surface state of both Ti 2p and O 1s are analysed by XPS and the value of the band gap of the semiconductor oxide estimated for all samples.

The photocatalytic activity in the gas phase degradation of NO_x is also investigated. Various processes are studied in the literature to abate the emissions of NO into the environment. The photocatalytic oxidation by a semiconductor, mainly TiO_2, is very promising and the tailoring of its features may promote the efficiency of the process.

Experimental

All the chemicals were of reagent grade purity and were used without further purification; bi-distilled water passed through a Milli-Q apparatus was used to prepare solutions and suspensions.

Sample Preparation

The sol–gel precursor (T), obtained by the hydrolysis ($t = 90$ min, $T = 65$ °C) of a solution of $Ti(OC_3H_7)_4$ and 2-propanol (water/alkoxide molar ratio = 49 and water/propanol molar ratio = 15) was dried as a xerogel [21]. A fraction of precursor was treated at 300 °C for 5 h in O_2 flux (T_300); the remaining part of the precursor was submitted to either pulsed (Bandelin, Ti horn, 20 kHz) for 1 h, or continuous (NTS Italia, Ti horn, 20 kHz) ultrasound water treatment for 30 min. The acoustic intensity, as determined calorimetrically, is 9 W cm^{-2} for continuous and 140 W cm^{-2} (maximum value) for pulsed ultrasound.

In the case of PW treatment, two acoustic intensities were used: 49 and 84 W cm^{-2} (35% and 60% of the maximum intensity, respectively). See Table 1 for the experimental parameters of the acoustic treatment.

Three samples were obtained during the growth assisted by pulsed ultrasound, by varying both the "time on" and the acoustic intensity ($TP_{0.5on}$49W, $TP_{0.9on}$49W, and $TP_{0.5on}$84W). The sample obtained using continuous US treatment is labeled TC9W.

Sample Characterization

Room-temperature X-ray powder diffraction (XRPD) patterns were collected with a Siemens D500 diffractometer over the 2θ range 10°–80°, with a step scan of $\Delta 2\theta = 0.02°$, and a Cu $K\alpha$ radiation. Rietveld refinement has been performed using the GSAS software suite and its graphical interface EXPGUI [15].

Specific surface areas were determined by the classical BET procedure using a Coulter SA 3100 apparatus.

Scanning electron microscopy (SEM) photographs are acquired with a LEO 1430.

TEM samples were prepared by spreading a suspension of powder in ethylic alcohol onto a carbon coated copper grid. A Philips 400T electron microscope operated at 120 keV was used for imaging and for acquiring selected area electron diffraction (SAED) patterns.

Diffuse reflectance spectra of the powders were measured on UV–vis scanning spectrophotometer (Perkin Elmer, Lambda 35), which was equipped with a diffuse reflectance accessory. A TiO_2 thin film was placed into the sample holder on integrated sphere for the reflectance measurements. A "total white" Perkin Elmer reference

Table 1 General conditions adopted for the US treatment in suspension

	Instrumental features				Experimental conditions		
	US source	d_{horn} (cm)	S_{horn} (cm^2)	Acoustic intensity (W cm^{-2})	t (s)	E_{tot} (kJ)	E_{tot}/V (kJ L^{-1})
$TP_{0.5on}49W$	Pulsed	1.3	1.3	49	3600	117	470
$TP_{0.5on}84W$	Pulsed	1.3	1.3	84	3600	202	808
$TP_{0.9on}49W$	Pulsed	1.3	1.3	49	3600	210	840
TC9W	Continuous	5.6	24.6	9	1800	414	414

material was used as an internal reference. The experimental absorption versus lambda plot was elaborated by differentiation to better highlight the different optical features of the catalyst spectra.

X-ray photoelectron spectra were acquired in an M-probe apparatus (Surface Science Instruments). The source was a monochromatic Al $K\alpha$ radiation (1486.6 eV). The binding energies (BEs) were corrected for specimen charging by referencing the C 1s peak to 284.6 eV. For the background subtraction the Shirley's method was used [16]. The relevant fittings were performed using only Gaussian line shapes, without BE or FWHM (full width at half maximum) constraints. The accuracy of the reported BE can be estimated to be ±0.1 eV.

Photocatalytic Experiments

In the photocatalytic oxidation of nitrogen, oxide immobilized particulate TiO_2 layers (ca. 0.1 g) were prepared on glass sheets (7 cm^2) by deposition from a suspension of the oxide in isopropanol. The immobilized photocatalyst was placed into a pyrex glass reactor (with a volume of 20 L) and irradiated with an halogenide lamp (Jelosil, model HG500) emitting in the 340–400 nm wavelength range, with a nominal power of 500 W, at room temperature. The relative humidity was kept constant in all the runs (50%). Air, NO_x, and N_2 gas streams were mixed to obtain the desired NO_x concentration (400 ppb), inside the photoreactor. The photodegradation products concentrations (NO and NO_2) were continuously monitored by an online chemiluminescent analyzer (Teledyne Instruments M200E). The NO_x adsorption onto the TiO_2 layer was determined through dark experiments. Degradation time was limited to 120 min.

Results and Discussion

Acoustic waves are known to cause the following effects in liquids [10]: (1) activation of mass transport, (2) heating, and (3) cavitation, i.e., generation of bubbles, which then collapse, giving rise to high local temperatures and pressures. Consequently, the growth of an oxide assisted by ultrasound can be differently affected by diverging processes: (1) formation of additional nucleation centers in the vicinity of bubbles; (2) increased growth rate of the particles owing to accelerated mass transport; and (3) disintegration of aggregates and agglomerates of primary crystallites by the shock waves resulting from bubble collapse.

To evaluate separately the different effects provoked by US, in the present case both continuous and pulsed ultrasound were used during the aging of a TiO_2 precursor obtained by sol–gel reaction. Table 2 reports data concerning the synthesized samples. The specific surface area ranges from 215 to 280 m^2 g^{-1}. Sample T_300, not submitted to US treatment and calcined at 300 °C shows the lowest surface area. Variable effects are introduced by the different US treatments. Pulsed US, with the highest total energy per volume ($TP_{0.9on}49W$ and $TP_{0.5on}84W$, see Table 1), produce an increase in surface area even with respect to the untreated precursor. This suggests that, in these cases, the prevailing effect of the US treatment may be the disintegration of aggregates. The continuous US treatment, instead, provokes a slight reduction in the surface area, with respect to the precursor, which suggests either a more pronounced grain growth or a less dispersed sample. The total pore volume and size are not significantly affected by the US treatment (Fig. 1a). The sample showing the largest pore volume is the pulsed one ($TP_{0.5on}84W$), the increase concerning the largest pore sizes. All the samples are mesoporous; the shape of the N_2 adsorption hysteresis loops (Fig. 1b) changes from H2 (prevailing "bottleneck" shape) in the precursor sample (T) to a

Table 2 Quantitative phase composition (A = anatase, B = brookite) and BET surface area

Sample	US source	% A	% B	S_{BET}, m^2 g^{-1}
T	–	60.2	39.8	254
T_300	–	67.0	33.0	215
$TP_{0.5on}49W$	Pulsed	55.6	44.4	231
$TP_{0.5on}84W$	Pulsed	53.0	47.0	268
$TP_{0.9on}49W$	Pulsed	53.5	46.5	278
TC9W	Continuous	63.0	37.0	242

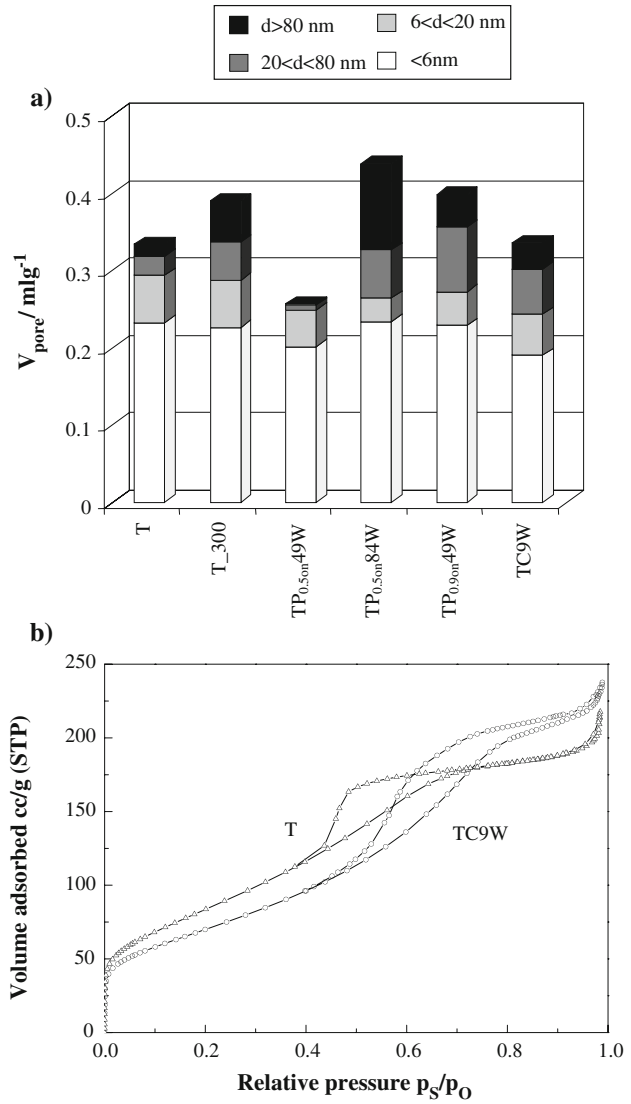

Fig. 1 **a** Distribution of pore volume of all samples and **b** BET isotherm, hysteresis loop of the precursor sample (T) and of the sample submitted to CW treatment

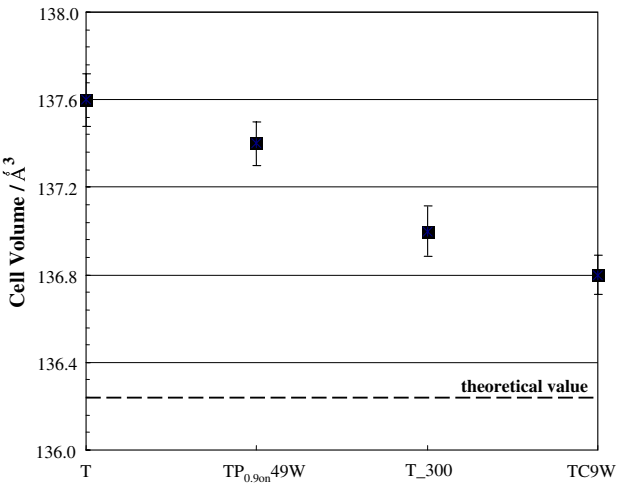

Fig. 2 Anatase cell volume of selected samples obtained by elaboration of experimental diffraction data

prevailing slit-shaped shape (H3) for the US-aged and thermally treated samples.

X-ray diffraction data show the presence of anatase and brookite polymorphs for all samples. The formation of the metastable brookite polymorph for small TiO_2 crystallite sizes is a well-established finding, often reported in the literature [21]. Pulsed US treatment promotes the formation of the brookite polymorph, particularly in the two samples showing the largest surface area. On the other hand, in the case of the CW US (sample TC9W), the treatment provokes a decrease in the brookite content of the sample. The thermal treatment at 300 °C (sample T_300) results in the lowest brookite content; the crystallite size, as estimated by the Sherrer's equation, applied to the breadth of the most intense anatase peak, is of 8 nm. The crystallite size for all the other samples is ranges around 4 nm.

Figure 2 reports the anatase cell volume as evaluated from X-ray diffraction data for selected samples. It is interesting to observe that, the CW US treatment leads to samples showing cell volumes closer to the theoretical values, indicating the formation of a more ordered and regular structure, even more ordered than the sample calcined at 300 °C but with no US treatment. It is worth observing that the US treatment provokes in any case a more regular spatial reticular organization since even the sample $TP_{0.9on}$49W, characterized by the largest surface area, shows a cell volume smaller than the precursor sample one.

Spectroscopic Characterization

To obtain information on the light absorption features of the various samples, experimental data of diffuse reflectance were elaborated to give absorption coefficient values $F(R)$ according to the Kubelka–Munk equation [16]. The corresponding band-gap values obtained by this procedure for all samples are reported in Table 3 (first column). The band gap values fall in the range expected for TiO_2 photocatalysts, with the only exception of the CW US sample, that shows a slightly higher value of band-gap with respect to the other ones. This point will be commented on further in the following.

Photodegradation of NO_x

Figure 3a displays the general trend of the NO_x degradation curves of some TiO_2 photocatalysts selected among those produced in the present study. The NO_x concentration

Table 3 Band gap values calculated by Kubelka–Munk equation of diffuse reflectance spectra and OH/O_{tot}, Ti^*/Ti^{4+} by XPS analysis for all samples

Sample	Band gap, eV	Ti^*/Ti^{4+}	OH/O_{tot}
T	3.19	–	0.17
T_300	3.20	–	0.12
$TP_{0.5on}49W$	3.13	–	0.29
$TP_{0.5on}84W$	3.16	–	0.26
$TP_{0.9on}49W$	3.18	–	0.21
TC9W	3.42	0.87	0.27

is the sum of the NO and NO_2 concentrations. The general mechanism for NO_x degradation by photocatalysis implies the oxidation of the nitric monoxide to nitric or nitrous acid induced by oxygen species produced at the TiO_2 surface [15]. The reaction path for NO_x conversion is generally mediated by OH radicals:

$$NO_2 + OH^\bullet \rightarrow HNO_3$$

$$NO + OH^\bullet \rightarrow HNO_2$$

In the present case, no increase in activity was observed upon increasing the catalyst amount. Therefore, it was concluded that only the exposed/external fraction of the catalyst was irradiated. All samples reach in a short time (30 min) a plateau region as concerns NO_x degradation, with values falling in a wide range: from 40% to about 90%.

The final sequence in efficiency, shown by the various samples, is displayed in Fig. 3b. It can be seen that the conversion of the precursor not submitted to sonication is very poor. All sonicated samples show better performances than the untreated T sample. Two US treated samples show the best conversions, higher than the thermally treated sample (T_300). In the case of the CW treated sample, the increase with respect to T_300 is significant (about 15%).

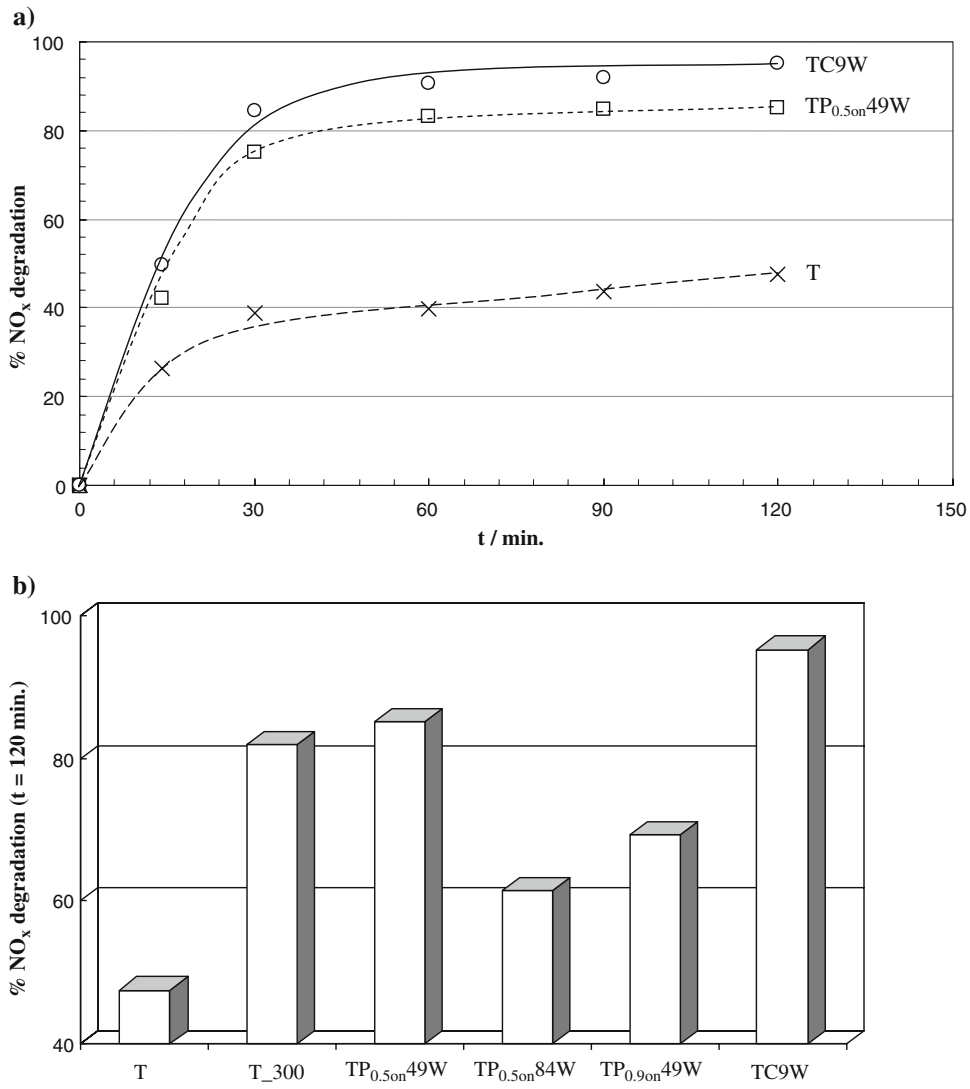

Fig. 3 **a** NO_x percent degradation as a function of reaction time for selected samples and **b** final percent degradation after 120 min for all the samples

An improvement of the photocatalytic efficiency of samples submitted to US treatment has been reported previously in the literature. Kim et al. [11], for example, observe an improvement in methylene blu degradation in samples submitted to US treatments. In general, the increase in the photocatalytic performance is attributed to an increase in the samples surface area, produced by the US treatment. This is not the case for the present samples, since those showing the best performances (TC9W and $TP_{0.5on}$ 49W) are the ones showing the lowest surface area, besides T_300. The interpretation of the origin of the better photocatalytic conversion is not straightforward. Further investigations of the surface state and of the microstructure may bring new evidence to elucidate the trend apparent in Fig. 3b.

XPS Analyses

The literature regarding XPS analyses of nanocrystalline TiO_2 samples obtained by ultrasound is not large, specifically concerning the region of Ti 2p. Yu et al. [5, 6] show no significant effects on the BE of Ti 2p (458.2 eV) in the case of nanosized TiO_2 powders obtained by sol–gel combined with US-treatment performed in a conventional ultrasonic bath. Gedanken et al. [7] measured the BE of Ti 2p at 457.1 eV in the case of un-calcined product and at 459.2 eV for the same sample calcined at 450 °C. The authors interpreted the shifts in the Ti 2p peak position, from the regular 458.2 eV, as due to the interaction of octadecylamine with TiO_2 in the templated synthesis of the mesoporous oxide [7].

Figure 4 shows the region of Ti 2p (a) and O 1s (b) of precursor (T) and CW US aged samples. In all samples, the peaks in the Ti 2p region are regular and the BEs (Ti $2p_{3/2}$ 458.3 eV) compare well with data of Ti(IV) in TiO_2 [15]. In the case, instead, of sample TC9W a second component (Ti*) at lower BE (Fig. 4a) can be appreciated (Table 3, second column). The presence of two components in the Ti 2p spectrum is not frequently observed in TiO_2 samples. Zhu et al. [22], reported this effect in TiO_2 particles prepared by a nonhydrolytic sol–gel reaction, without any US treatment. They attributed the component at lower BE to Ti(III). In the present case, the best fit of the Ti 2p region yields two components at 456.8 and at 458.3 eV, respectively. The component at lower BE might be interpreted, according to Zhu et al. [22], as due to the presence of defective titanium surface sites, these in turn being the result of the interactions of the oxide surface with the OH radicals produced by the CW US treatment. It is interesting to observe that TC9W is just the most photocatalytically performing sample with respect to the degradation of NO_x.

The O 1s peaks of the present samples show, in any case, a regular pattern (Fig. 4b) and show two components, corresponding, respectively, to oxygen in the oxide lattice

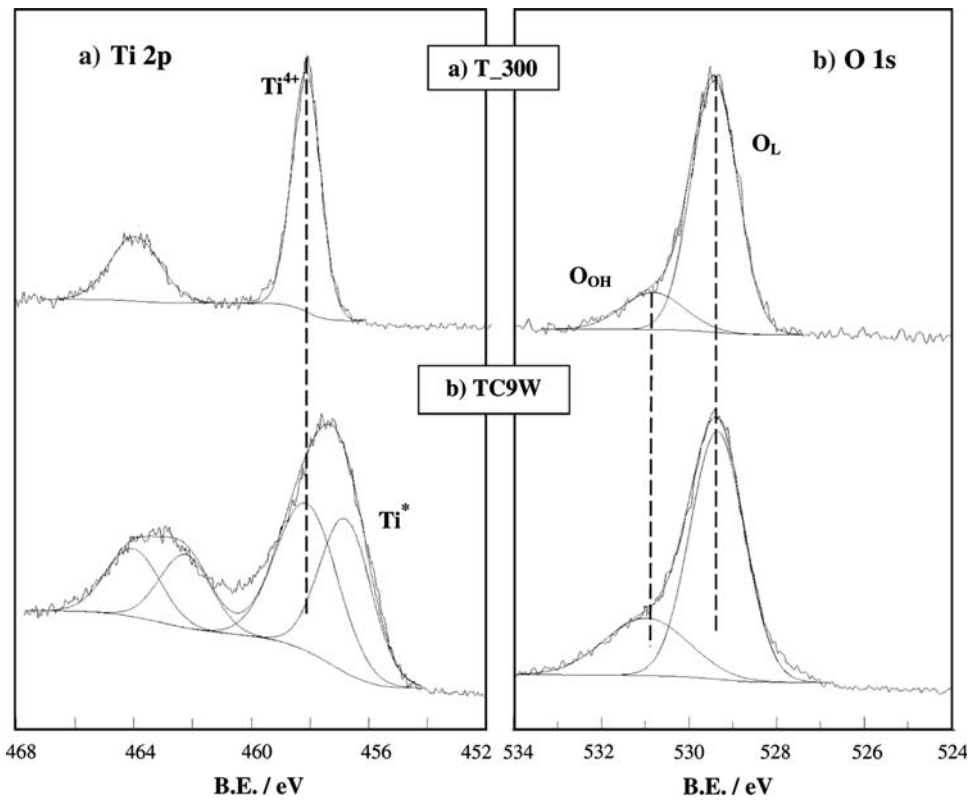

Fig. 4 XPS Ti 2p **a** and O 1s **b** regions for T_300 and TC9W

(O_L), and to surface hydroxyl (O_{OH}). The ratio between O_{OH} and total oxygen components ($O_{OH} + O_L$) is reported in Table 3 (third column) and can be considered as an indication of the degree of hydrophilicity of each sample [15]. The two samples showing top photocatalytic performances are the ones showing the highest OH/O_{tot} ratio.

SEM and TEM Observations

SEM images (Fig. 5) show that the samples submitted to US are, in general, more disperse than those obtained in the absence of US. The sample submitted to CW US, besides being much more disaggregated than the precursor, appears to be composed by smaller particles.

To obtain further indications concerning the microstructure of the samples, TEM images of the best photocatalysts were obtained and compared with those of the untreated precursor.

Figure 6a, referring to the untreated precursor sample (T), shows aggregates in which the size of the crystallites is extremely reduced. The figure also shows the typical microstructure of this sample and in the SAED pattern the presence of reflections due to anatase and brookite phases, although largely overlapping, appear clearly, in agreement with the XRD data in Table 1. The diffraction rings are uniform and with homogeneous intensity supporting the nanometric size of the crystallites and their spatial isotropy.

The microstructure of the pulsed sample ($TP_{0.5on}49W$) is shown in Fig. 6b. The SAED pattern, also in this case, supports the presence of the two TiO_2 polymorphs. Crystallite clusters appear to be relatively dense, so that only the peripheric regions can be analysed in detail. Crystallite size even in this case compares well with the XRD value.

The microstructure of the TC9W sample is shown in Fig. 6c. Also in this case the presence of the A and B polymorphs is well appreciable in the SAED spectrum. In the case of this sample, the crystallite agglomerates appear to be densely packed, possibly as a consequence of their reduced size, which can be estimated to be around 1–2 nm. The crystallites appear to be rather homodisperse concerning both shape and size. The extremely small size of the crystallites would justify the larger value of the band gap of this sample and the relevant blue shift, reported by other researchers for very small crystallite sizes [13].

Conclusions

Two main features, promoted by US treatments, can be assumed to support a better photocatalytic performance: reduction in the crystallite sizes and larger surface coverage by OH.

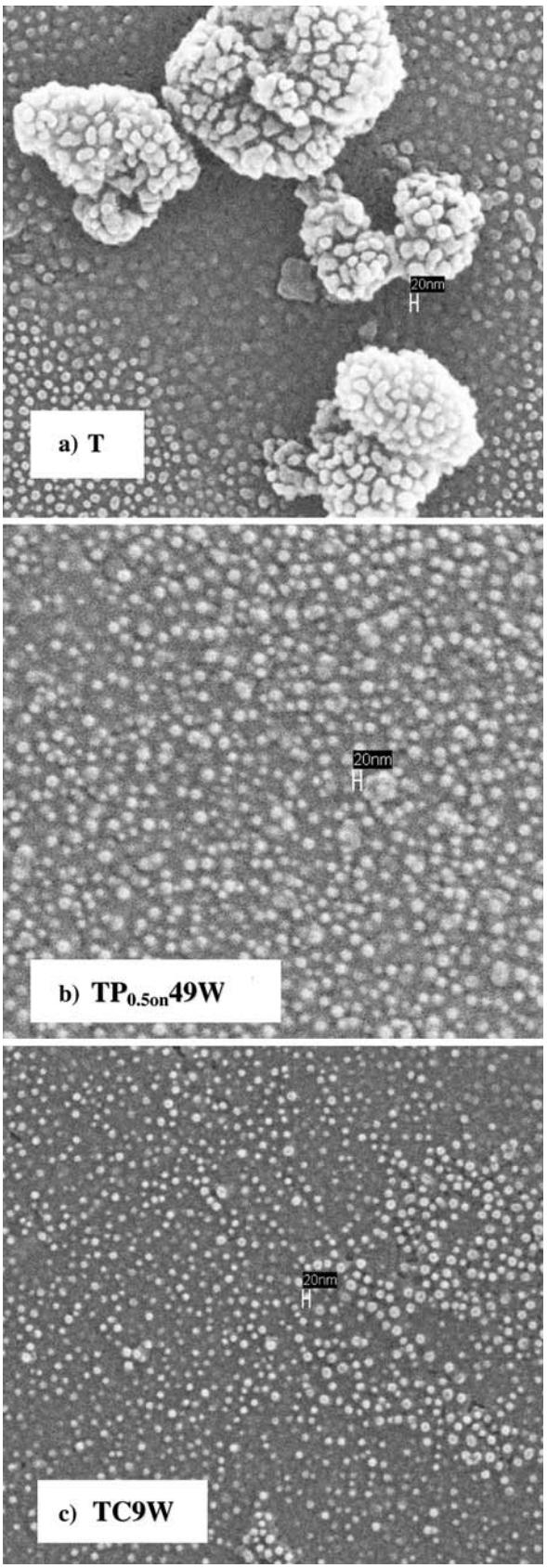

Fig. 5 SEM images of the precursor sample (T) and of the two best active US treated samples ($TP_{0.5on}49W$ and TC9W)

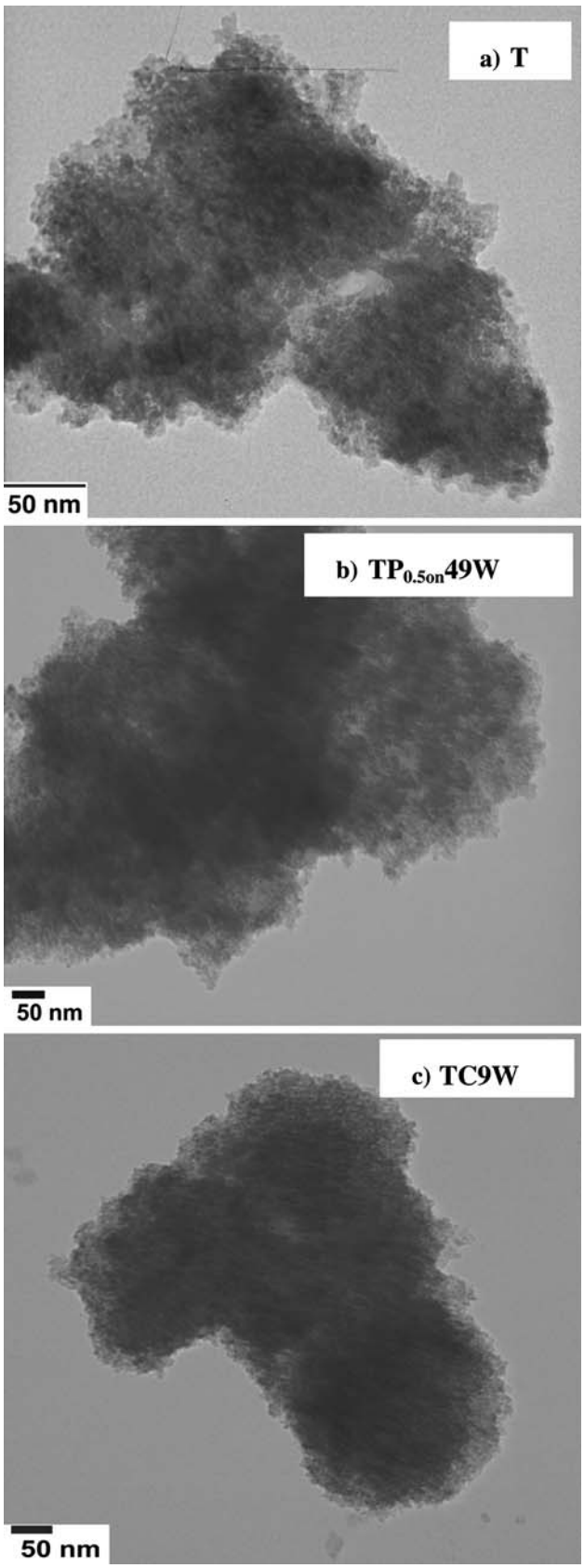

Fig. 6 TEM images of the precursor sample (T) and of the two best active US treated samples ($TP_{0.5on}49W$ and TC9W)

Reduction in the crystallite size of a semiconductor can usually lead to enhancement in the photocatalytic degradation. It is believed that enhanced quantum yields are achievable for the nanosized catalysts due to more efficient transfer of the photogenerated charge carriers from the interior to the particle surface [23]. Moreover, in these catalysts the very small size of the crystallites is also accompanied by a more ordered crystalline structure and the samples appear to be more regular and can be considered to contain a relatively low concentration of lattice defects. These features result in a lower recombination rate between electrons and holes and, therefore, in an overall better photocatalytic performance.

The OH population of the surface is a key feature in NO_x photodegradation [15]; a more hydroxylated surface promotes both the formation of OH radicals and also the adsorption of the pollutant molecules prior to the degradation.

The analysis of the present data seems to suggest that the relevant parameter imposing the final features of the oxides is the US total energy *per* volume (E_{tot}/V) and not the acoustic intensity or the pulsed or continuous mode of US. The two samples obtained at the higher E_{tot}/V (808, 840 kJ L^{-1}) show the largest surface area and highest brookite content. The other way round, the two samples obtained at around half E_{tot}/V (414, 470 kJ L^{-1}) show very similar features between each other and display the top photocatalytic activity. The continuous mode induces, further, the presence of surface defects and consequently yields the best photocatalyst.

Acknowledgment This research has been supported by the Ministry of Education, University and Research (MIUR, FIRST Funds).

References

1. C. Petrier, D.J. Casadonte, *Advances in Sonochemistry*, vol. 6 (JAI Press, London, 2001), pp. 91–110
2. G. Zhang, I. Hua, Environ. Sci. Technol. **34**(8), 1529 (2000). doi:10.1021/es981127f
3. C. Petrier, A. Jeunet, J.L. Luche, G. Reverdy, J. Am. Chem. Soc. **114**, 3148 (1992). doi:10.1021/ja00034a077
4. A. Kotronarou, G. Mills, M. Hoffmann, Environ. Sci. Technol. **26**(7), 1460 (1992). doi:10.1021/es00031a026
5. L. Wu, J.C. Yu, L. Zhang, X. Wang, W. Ho, J Solid State Chem. **177**, 2584 (2004). doi:10.1016/j.jssc.2004.03.033
6. J.C. Yu, J. Yu, L. Zhang, W. Ho, J. Photochem. Photobiol. A: Chem. (Easton) **148**, 263 (2002)
7. Y. Wang, S. Chen, X. Tang, O. Palchik, A. Zaban, Y. Koltypin, A. Gedanken, J. Mater. Chem. **11**, 521 (2001). doi:10.1039/b006070o
8. H. Arami, M. Mazloumi, R. Khalifehzadeh, S.K. Sadrnezhaad, Mater. Lett. **61**, 4559 (2007). doi:10.1016/j.matlet.2007.02.051
9. Y. Wang, X. Tang, L. Yin, W. Huang, Y. Rosenfeld Hacohen, A. Gedanken, Adv. Mater. **12**, 1183 (2000). doi :10.1002/1521-4095(200008)12:16<1183::AID-ADMA1183>3.0.CO;2-X

10. P.E. Meskin, A.E. Baranchikov, V.K. Ivanov, D.R. Afanasev, A.I. Gavrilov, B.R. Churagulov, N.N. Oleinikov, Inorg. Mater. **40**, 1058 (2004). doi:10.1023/B:INMA.0000046468.73127.f5
11. S.Y. Kim, T.S. Chang, C.H. Shin, Catal. Lett. **118**, 224 (2007). doi:10.1007/s10562-007-9174-x
12. J. Yu, J.C. Yu, M.K.-P. Leung, W. Cheng, B. Ho, X. Zhao, J. Zhao, J. Catal. **217**, 69 (2003)
13. H. Lin, C.P. Huang, W. Li, C. Ni, S. Ismat Shah, Y.-H. Tseng, Appl. Catal. B **68**, 1 (2006). doi:10.1016/j.apcatb.2006.07.018
14. S. Bakardjieva, V. Stengl, L. Szatmary, J. Subrt, J. Lukac, N. Murafa, D. Niznansky, K. Cizek, J. Jirkovskyc, N. Petrova, J. Mater. Chem. **16**, 1709 (2006). doi:10.1039/b514632a
15. S. Ardizzone, C.L. Bianchi, G. Cappelletti, S. Gialanella, C. Pirola, V. Ragaini, J. Phys. Chem. C **111**, 13222 (2007). doi:10.1021/jp0741096
16. G. Cappelletti, C.L. Bianchi, S. Ardizzone, Appl. Catal. Environ. **78**, 193 (2008). doi:10.1016/j.apcatb.2007.09.022
17. J. Šícha, D. Heřman, J. Musil, Z. Strýhal, J. Pavlík, Nanoscale Res. Lett. **2**(3), 123 (2007). doi:10.1007/s11671-007-9042-z
18. V. Vega, V.M. Prida, M. Hernández-Vélez, E. Manova, P. Aranda, E. Ruiz-Hitzky, M. Vázquez, Nanoscale Res. Lett. **2**(7), 355 (2007). doi:10.1007/s11671-007-9073-5
19. S. Watson, D. Beydoun, J. Scott, R. Amal, J. Nanopart. Res. **6**(2), 193 (2004). doi:10.1023/B:NANO.0000034623.33083.71
20. J. Rajeswari, P.S. Kishore, B. Viswanathan, T.K. Varadarajan, Nanoscale Res. Lett. **2**(10), 496 (2007). doi:10.1007/s11671-007-9088-y
21. T. Boiadjieva, G. Cappelletti, S. Ardizzone, S. Rondinini, A. Vertova, Phys. Chem. Chem. Phys. **6**, 3535 (2004). doi:10.1039/b402370f
22. J. Zhu, J. Yang, Z.F. Bian, J. Ren, Y.-M. Liu, Y. Cao, H.-X. Li, H.-Y. He, K.-N. Fan, Appl. Catal. B Environ. **76**, 82 (2007). doi:10.1016/j.apcatb.2007.05.017
23. M. Benmami, K. Chhor, A.V. Kanaev, J. Phys. Chem. B **109**(42), 19766 (2005). doi:10.1021/jp051396+